Optical bistability in a doubly resonant $\chi^{(2)}$-nonlinear plasmonic nanocavity

Andreas Hänsel, Oleg A. Egorov, Shakeeb Bin Hasan,* Carsten Rockstuhl, and Falk Lederer
Institute of Condensed Matter Theory and Solid State Optics, and Abbe Center of Photonics, Friedrich-Schiller-Universität Jena, Max-Wien-Platz 1, 07743 Jena, Germany
(Received 29 March 2012; published 31 May 2012)

We demonstrate optical bistability in a $\chi^{(2)}$-nonlinear plasmonic nanocavity. The nanocavity is made from a metal-insulator-metal waveguide possessing stubs as realistic mirrors. The design of the nanocavity is sufficiently flexible to allow for resonances at both the fundamental and the second-harmonic frequency and a phase-matched nonlinear interaction. By using rigorous diffraction theory and a mean-field approach, we establish the conditions required to observe optical bistability and present optimal configurations with regard to a minimum pump power. This work might be useful for employing plasmonic nanocircuits in optical computing schemes.

DOI: 10.1103/PhysRevA.85.053843 PACS number(s): 42.65.Pc, 73.20.Mf, 42.65.Ky

I. INTRODUCTION

The ability of plasmonic nanowaveguides to localize light well beyond its diffraction limit makes them promising constituents for many useful functional devices. A referential application that triggered many research efforts is that of optical computing using integrated plasmonic nanocircuits. It would constitute a paradigm shift since it promises to nullify performance limitations of ordinary electronic computers in terms of processing speed, element size, and element integration [1,2]. To transfer such applications from the realm of fantasy to real-world devices, however, many obstacles have to be overcome. At the moment, basic building blocks are urgently required that allow implementation of complex logical elements.

A plasmonic nanodevice possessing a bistable response is one such basic building block. The bistability suggests that for a certain input power the output power may attain two different values, depending upon the operational past of the device. Such a bistable device can be used to implement all-optical logical functions such as transistors, optical memories, and may provide clipping and limiting actions. A typical bistable device consists of an optical resonator (Fabry-Perot) comprising a medium with a nonlinear response. While considering materials with a $\chi^{(2)}$ nonlinearity, only conventional microcavities, i.e., microcavities made from dielectric materials, have been discussed so far. However, they cannot be scaled down to nanometric dimensions and their integration into plasmonic nanocircuits is therefore out of reach. Nonetheless, they were instrumental in the study of many basic effects such as second-harmonic generation [3,4] or optical parametric oscillation [5]. The main problem to solve while realizing cavities with a $\chi^{(2)}$ nonlinearity is the compensation of the phase velocity mismatch between fundamental harmonic (FH) and second harmonics (SH). The phase mismatch not only substantially reduces the nonlinear interaction between the involved harmonics but also renders the realization of a doubly resonant microcavity to be very difficult [4]. Therefore, the future development of bistable plasmonic devices suitable for integration into nanocircuits requires particular attention to the aspect of achieving a phase-matched interaction in a doubly resonant nanocavity.

In the present study, we suggest a method for solving this issue. We present a bistable doubly resonant plasmonic nanocavity possessing an instantaneous $\chi^{(2)}$ nonlinear response and assuring phase matching. In the design process we strictly consider natural available materials so that the bistable device is amenable to fabrication. The main body of our suggested nanocavity is made of a metal-insulator-metal (MIM) plasmonic nanowaveguide where a $LiNbO_3$ layer is sandwiched between two Ag layers [1]. The nanocavity is formed by using stub mirrors which are well known at microwave frequencies. This concept has been recently introduced into plasmonic MIM waveguides [6,7]. The key element in our design is that each mirror consists of two stubs (see Fig. 1). Each of them is almost transparent for one frequency and strongly reflects the other one. Controlling the spacing between both stubs permits offsetting the phase mismatch of the waves at both frequencies per round trip. Thus this nanocavity design resembles the ideas of a chirped mirror as used to generate ultrashort pulses. There, different frequency components are back reflected at different positions along the spatially extended mirror. In passing, we note that contrary to an intrinsic optical bistability in resonant nonlinear materials that exploit a first-order phase transition (for example, see [8]), the materials we consider here are not resonant.

Since the resulting bistable device shall additionally be driven with pump powers as small as possible, an optimal design requires a careful balance of various aspects. On the one hand, the nanocavity should be as long as possible to allow for an efficient nonlinear interaction. On the other hand, a large nanocavity can lower the finesse, since dissipation of the surface plasmon polaritons prevents the efficient buildup of a field. To provide analytical insights into the problem, we therefore derive explicit analytical expressions that allow predicting the optimal parameters to observe optical bistability at minimal input pump powers. With this work we attempt to provide the necessary means to design bistable plasmonic nanocavities using $\chi^{(2)}$-nonlinear materials that could potentially be used in the future for many applications mentioned above.

II. ANALYSIS

The full description of the properties of the nanocavity has necessarily to begin with Maxwell's equations. They are used to calculate the modal field profile of the MIM waveguide, their

*Corresponding author: shakeeb-bin.hasan@uni-jena.de

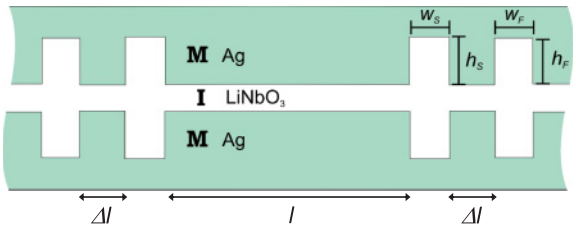

FIG. 1. (Color online) Schematic of the plasmonic cavity. The stub mirrors for the fundamental (outer stubs) and second harmonics (inner stubs) allow for tuning both frequencies independently.

dispersion relations, and in addition, the reflection coefficients of the nanocavity mirrors [9]. Without loss of generality, we assume in the following a vacuum wavelength for the FH of $\lambda^{\mathrm{F}} = 1.55\,\mu$m and for the corresponding SH of $\lambda^{\mathrm{S}} = \lambda^{\mathrm{F}}/2$. The MIM waveguide is made from metal films sufficiently thick such that the boundary effects are negligible and the fields in the waveguide will correspond to those for semi-infinite metals. The dielectric layer is made up of $LiNbO_3$, which is 150 nm thick and whose optical axis is aligned to the x axis of Fig. 1. The thickness was purposely chosen such that only the symmetric plasmonic mode (with respect to the magnetic field) at both frequencies is supported [1]. The complex modal propagation constant $\beta_0 = \beta_0' + i\alpha_0/2$ of this mode is defined implicitly by the following transcendental equation [1]:

$$\tanh\left(\sqrt{\beta_0^2 - k_0^2\epsilon_m}d\right) = -\frac{\sqrt{\beta_0^2 - k_0^2\epsilon_d}\epsilon_m}{\sqrt{\beta_0^2 - k_0^2\epsilon_m}\epsilon_d} \qquad (1)$$

where ϵ_m and ϵ_d denote the permittivities of metal and dielectric, respectively, $k_0 = 2\pi/\lambda$ and d being the thickness of the dielectric layer.

To quantify the optical properties of the stub mirrors, the complex reflection and transmission coefficients have been computed using COMSOL MULTIPHYSICS, which solves Maxwell's equations using finite element method [10–12] while relying on tabulated values for the dielectric functions of all materials involved [13,14]. The strategy of optimizing the mirrors consists of two steps. First, by changing the widths $w_{\mathrm{F}}, w_{\mathrm{S}}$ and heights $h_{\mathrm{F}}, h_{\mathrm{S}}$ of each individual stub mirror one can compute the reflection coefficient at both harmonics independently [see Figs. 2(a) and 2(b)]. We found that a few configurations can provide high reflectivity with $R_{\max} > 0.95$.

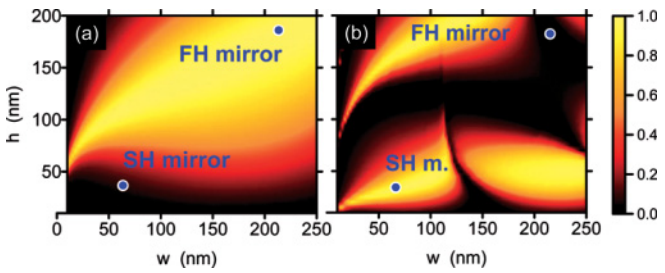

FIG. 2. (Color online) Reflectivities for FH (a) and SH (b). The dimensions of the stubs are chosen as 215 nm × 180 nm and 57.5 nm × 30 nm for the FH and SH mirrors, respectively. It can be clearly seen that these mirrors are highly reflective at either the FH or the SH frequency while the other frequency is left unaffected.

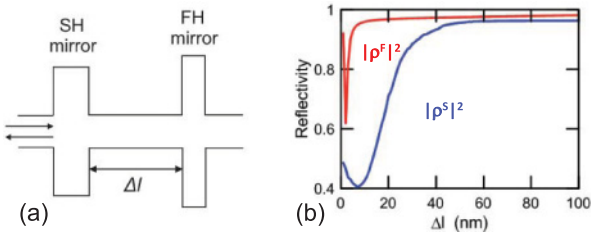

FIG. 3. (Color online) (a) Sketch of the composite mirror for both harmonics. (b) Reflectivities $|\rho_0^{\mathrm{F}}|^2$ for FH and $|\rho_0^{\mathrm{S}}|^2$ for SH of the composite mirror depending on the stub separation Δl.

In order to tune the nanocavity at each frequency individually, we have chosen mirrors that are highly reflective at one frequency whereas they are transparent at the other. This was done on purpose to ensure that the spatial separation of the FH and SH mirrors Δl can be used to compensate for the phase mismatch. This is possible since the different frequencies will experience a nanocavity of different geometrical but identical optical lengths. This allows achieving a resonance at both harmonics in a single configuration. However, the separation between the two stubs forming the composite mirror also has to be large enough such that near-field interaction among neighboring stub mirrors is reduced to negligible and they regain their response when placed in isolation. Therefore, we calculated in a second step the complex reflection coefficient of the composite mirror [Fig. 3(b)] for both FH ($|\rho_0^{\mathrm{F}}|^2$) and SH ($|\rho_0^{\mathrm{S}}|^2$), depending on the separation between two stubs Δl. It turned out that for $\Delta l > 50$ nm, both mirrors can be treated independently [Fig. 3(b)]. The reflection coefficient of the composite mirror agreed with that for an isolated single stub. These complex reflection coefficients of the composite stubs are considered in the subsequent analysis of the bistable response.

To analyze the output power depending on the input power at the FH frequency, we use the coupled-mode theory for lossy systems (see Appendix). Ignoring group velocity dispersion, the standard equations for the slowly varying amplitudes $u^{\{\mathrm{F,S}\}}$ of forward- and backward-propagating modes at FH and SH can be written as [15,16]

$$\begin{aligned} \pm i\frac{\partial u_\pm^{\mathrm{F}}}{\partial z} + \frac{i}{v_g^{\mathrm{F}}}\frac{\partial u_\pm^{\mathrm{F}}}{\partial t} + i\frac{\alpha_0^{\mathrm{F}}}{2}u_\pm^{\mathrm{F}} + \chi_{\mathrm{eff}}^{(2)}(u_\pm^{\mathrm{F}})^\star u_\pm^{\mathrm{S}}\exp(-i\Delta\beta z) = 0 \\ \pm i\frac{\partial u_\pm^{\mathrm{S}}}{\partial z} + \frac{i}{v_g^{\mathrm{S}}}\frac{\partial u_\pm^{\mathrm{F}}}{\partial t} + i\frac{\alpha_0^{\mathrm{S}}}{2}u_\pm^{\mathrm{S}} + \chi_{\mathrm{eff}}^{(2)}(u_\pm^{\mathrm{F}})^2\exp(i\Delta\beta z) = 0 \end{aligned} \qquad (2)$$

where v_g denotes the group velocity defined by $v_g^{-1} = \partial\beta'/\partial\omega|_{\omega=\omega_0}$, the subscripts $(+)$ and $(-)$ denote the forward- and backward-propagating modes, while the superscripts (F) and (S) stand for FH and SH, respectively. The nonlinear phase mismatch factor between the FH and SH is represented by $\Delta\beta = 2\beta_0'^{\mathrm{F}} - \beta_0'^{\mathrm{S}}$, whereas $\chi_{\mathrm{eff}}^{(2)}$ is the nonlinear coupling coefficient defined under Kleinman symmetry (details are documented in the Appendix). Due to strong light localization in the MIM waveguide, the effective nonlinear coefficient $\chi_{\mathrm{eff}}^{(2)}$ can be an order of magnitude larger than in conventional dielectric waveguides. Equations (2) take into account the propagation losses of the MIM waveguides, which are related

to the damping lengths $(\alpha^{\mathrm{F}})^{-1} \approx 31\ \mu$m, $(\alpha^{\mathrm{S}})^{-1} \approx 17.5\ \mu$m for the FH and SH modes, respectively. Thus, the resonator length l shall be substantially smaller than these damping lengths. This entails, on the other hand, that the cavity length will be also much less than the coherence length

$$L_c = \frac{2\pi}{\Delta\beta}.$$

Therefore, the phase mismatch term $\Delta\beta$ can be neglected in Eqs. (2) but it will be taken into account by the appropriate boundary conditions at the mirrors. They read as

$$\begin{aligned} u_+^{\mathrm{F}}(0) &= \rho_0^{\mathrm{F}} \exp\left[i\left(l\beta_0'^{\mathrm{F}} + 2\beta_0'^{\mathrm{F}}\Delta l + \varphi_0^{\mathrm{F}}\right)\right] u_-^{\mathrm{F}}(0) + t^{\mathrm{F}}\sqrt{P}, \\ u_+^{\mathrm{S}}(0) &= \rho_0^{\mathrm{S}} \exp\left[i\left(l\beta_0'^{\mathrm{S}} + \varphi_0^{\mathrm{S}}\right)\right] u_-^{\mathrm{S}}(0), \\ u_-^{\mathrm{F}}(l) &= \rho_0^{\mathrm{F}} \exp\left[i\left(l\beta_0'^{\mathrm{F}} + 2\beta_0'^{\mathrm{F}}\Delta l + \varphi_0^{\mathrm{F}}\right)\right] u_+^{\mathrm{F}}(l), \\ u_-^{\mathrm{S}}(l) &= \rho_0^{\mathrm{S}} \exp\left[i\left(l\beta_0'^{\mathrm{S}} + \varphi_0^{\mathrm{S}}\right)\right] u_+^{\mathrm{S}}(l). \end{aligned} \tag{3}$$

Here, P denotes the external pump power per unit width and $t^{\mathrm{F}} \approx \sqrt{1 - |\rho_0^{\mathrm{F}}|^2}$. Because the resonator length l is sufficiently small so that nonlinear changes and damping are also small upon round trip, we can further simplify our analysis by deriving mean-field equations (for details see [15,16]). The equations for the normalized FH b_1 and SH output b_2 are

$$\begin{aligned} \frac{\partial b_1}{\partial T} + (i + \Delta_1) b_1 + b_1^* b_2 &= E_0, \\ \frac{\partial b_2}{\partial T} + (i\delta + \Delta_2) b_2 + b_1^2 &= 0, \end{aligned} \tag{4}$$

respectively, where the evolution time T is scaled with respect to FH photon lifetime τ_{ph} defined as

$$\tau_{\mathrm{ph}} = \left(\frac{1 + \left(\rho_0^{\mathrm{F}}\right)^2 e^{-\alpha_0^{\mathrm{F}} l}}{1 - \left(\rho_0^{\mathrm{F}}\right)^2 e^{-\alpha_0^{\mathrm{F}} l}}\right) l \left(v_g^{\mathrm{F}}\right)^{-1},$$

whereas δ is the ratio of the photon lifetimes of FH and SH:

$$\delta = \frac{v_g^{\mathrm{S}}\left(1 - \left|\rho_0^{\mathrm{S}}\right|^2 e^{-\alpha_0^{\mathrm{S}} l}\right)}{v_g^{\mathrm{F}}\left(1 - \left|\rho_0^{\mathrm{F}}\right|^2 e^{-\alpha_0^{\mathrm{F}} l}\right)}.$$

In the stationary limit $(\partial/\partial T) = 0$, Eq. (4) simplifies to

$$\begin{aligned} (i + \Delta_1)\, b_1 + b_1^* b_2 &= E_0, \\ (i\delta + \Delta_2)\, b_2 + b_1^2 &= 0. \end{aligned} \tag{5}$$

In passing, we note that we have included the different effective resonator lengths for both frequencies. The detunings of both fields from the respective cavity resonances are

$$\Delta_1 = -\frac{1 + \left|\rho_0^{\mathrm{F}}\right|^2 e^{-\alpha_0^{\mathrm{F}} l}}{1 - \left|\rho_0^{\mathrm{F}}\right|^2 e^{-\alpha_0^{\mathrm{F}} l}} \left((l + 2\Delta l)\beta_0'^{\mathrm{F}} + \varphi_0^{\mathrm{F}} - m\pi\right), \tag{6}$$

$$\Delta_2 = -\frac{v_g^{\mathrm{S}}\left(1 + \left|\rho_0^{\mathrm{F}}\right|^2 e^{-\alpha_0^{\mathrm{F}} l}\right)}{v_g^{\mathrm{F}}\left(1 - \left|\rho_0^{\mathrm{F}}\right|^2 e^{-\alpha_0^{\mathrm{F}} l}\right)} \left(l\beta_0'^{\mathrm{S}} + \varphi_0^{\mathrm{S}} - n\pi\right). \tag{7}$$

These cavity detunings become zero at resonance, which practically means that the phase shift of the intracavity waves becomes a multiple of 2π (m,$n = 0,1,2\ldots$) after one complete round trip between the mirrors. Keeping the cavity length smaller than the nonlinear coherence length, a clear advantage of the proposed composite stub mirror is the possibility to change separation Δl between FH and SH stubs independent of the effective cavity length l. Indeed, the two parameters l and Δl can be tuned to achieve the resonance condition for both harmonics ($\Delta_{1,2} = 0$). We note that the phase mismatch between the two harmonics can also be compensated by the phase shift due to the reflection at mirrors:

$$2\varphi_0^{\mathrm{F}} - \varphi_0^{\mathrm{S}} + \Delta\beta l + 4\beta_0'^{\mathrm{F}}\Delta l = 2\pi q,$$

with $q = 0,1,2,\ldots$.

The parameter E_0 in Eqs. (4) denotes the normalized amplitude of the input pump mode, which is related to the actual pump power as

$$E_0 = i\chi_{\mathrm{eff}}^{(2)} l \frac{\left|1 + \left(\rho_0^{\mathrm{F}}\right)^2 \rho_0^{\mathrm{S}}\right|}{\left[1 - \left(\rho_0^{\mathrm{F}}\right)^2 e^{-\alpha_0^{\mathrm{F}} l}\right]^2} \sqrt{\frac{v_g^{\mathrm{S}}\left[1 + \left(\rho_0^{\mathrm{F}}\right)^2 e^{-\alpha_0^{\mathrm{F}} l}\right]}{v_g^{\mathrm{F}}\left[1 + \left(\rho_0^{\mathrm{S}}\right)^2 e^{-\alpha_0^{\mathrm{S}} l}\right]}}\, t^{\mathrm{F}}\sqrt{P}. \tag{8}$$

Because of the propagation losses, the finesse of the cavity decreases with increasing length l. On the other hand, the nonlinear effects accumulate during propagation and, therefore, they are proportional to this length. Hence there is an optimal cavity length which shall provide a minimal threshold for the nonlinear effects.

Searching for the optimal conditions for optical bistability, we proceed with an analysis of the mean-field equations (4). Rewriting them for the intensities of the stationary solutions, one obtains [16,17]

$$\begin{aligned} &\left[|b_1|^4 + 2(\delta - \Delta_1\Delta_2)|b_1|^2 + \left(\Delta_1^2 + 1\right)\left(\Delta_2^2 + \delta^2\right)\right]|b_1|^2 \\ &\quad = \left(\Delta_2^2 + \delta^2\right) E_0^2 \end{aligned} \tag{9}$$

and

$$|b_2| = \frac{|b_1|^2}{\sqrt{\Delta_2^2 + \delta^2}}. \tag{10}$$

Equation (9) has three real and positive solutions for the intensity $|b_1|^2$, provided that the conditions

$$\frac{|\Delta_2|(|\Delta_1| - \sqrt{3})}{(\sqrt{3}|\Delta_1| + 1)} > \delta$$

and

$$\Delta_1\Delta_2 > 0$$

hold. According to the above conditions, it is necessary that both detunings be nonzero and the FH detuning Δ_1 exceeds $\sqrt{3}$. As a result, the input-output response of the resonator is S shaped [Fig. 4(a)]. The bistable input-output curve possesses two limit points $|E_0|^2 = |E_\pm|^2$ (Fig. 2), determined by the condition

$$\partial|E_0|^2/\partial|b_1|^2 = 0$$

[see Fig. 4(a)], where the corresponding values of the intracavity intensities $|b_\pm|^2$ are

$$\begin{aligned} |b_\pm|^2 = \big[&2(\Delta_1\Delta_2 - \delta) \\ &\pm\sqrt{4(\delta - \Delta_1\Delta_2)^2 - 3\left(\Delta_1^2 + 1\right)\left(\Delta_2^2 + \delta^2\right)}\big]/3. \end{aligned} \tag{11}$$

Inserting $|b_\pm|^2$ into Eq. (9), one obtains the values of the normalized pump intensities $|E_\pm|^2$ required for optical

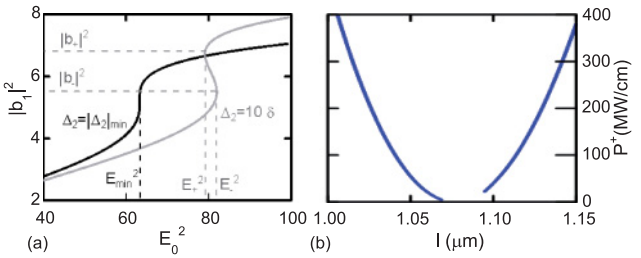

FIG. 4. (Color online) (a) The intracavity intensity of the FH vs the normalized pump intensity Eq. (9) for different frequency detunings Δ_2 and constant detuning $\Delta_1 = 2.45$. $|b_\pm|^2$ and $|E_\pm|^2$ designate the limit points of optical bistability. (b) Intensity of the external pump field $P_\pm$ for the limit point of optical bistability vs cavity length l and fixed $\Delta l = 74$ nm.

bistability. These values depend strongly on the detunings $\Delta_{1,2}$. Then, varying the detunings as independent parameters and looking for the extrema of the obtained equations, we calculated the minimal intensity of the pump beam required for the observation of optical bistability:

$$E_{\min}^2 = \frac{64(7+3\sqrt{5})}{27(\sqrt{5}-1)}\delta \approx 26.29\delta. \tag{12}$$

These values were obtained for the following optimal FH and SH detunings:

$$\begin{aligned} |\Delta_1|_{\min} &= (2+\sqrt{5})/\sqrt{3} \approx 2.45, \\ |\Delta_2|_{\min} &= \sqrt{3}(3+\sqrt{5})\delta/(\sqrt{5}-1) \approx 7.34\delta. \end{aligned} \tag{13}$$

The absolute theoretical minimum for the pump intensity corresponds to the point of the nascent bistability, in other words, the boundaries in the parameter plane between the monostable and multistable response of the cavity [see the curve with $|\Delta_2|_{\min}$ in Fig. 4(a)]. By using Eq. (12) together with Eq. (8), we can express the minimum power required for observing bistability as

$$P_{\min} \approx \frac{\left(1-\left|\rho_o^F\right|^2 e^{-\alpha_0^F l}\right)^4 v_g^F}{\left(2l\,\chi_{\text{eff}}^{(2)}\right)^2\left(1-\left|\rho_o^F\right|^2\right)v_g^S}|E_{\min}|^2. \tag{14}$$

Using Eqs. (6)–(9), one can easily express the power required for bistability in terms of the real system parameters of the cavity. In the vicinity of a longitudinal (Fabry-Perot) resonance, the power for optical bistability ($|P_\pm|^2$) is very sensitive to the resonator length l [Fig. 4(b)]. Note that in accordance with the mean-field result (9), there are no real solutions for the pump power when the cavity is exactly tuned to the resonance either for FH or SH. By changing the separation between FH and SH stubs of the composite mirrors one can achieve the conditions for the optimal detuning given by Eq. (13) and obtain the minimal value of the pump power. For instance, a cavity with a resonator length of $l \approx 478$ nm and $\Delta l \approx 54$ nm reaches the minimal value of the pump power $P_{\min}$, shown in Fig. 5(a). Such optimal parameters can be found for any longitudinal resonance [for different values of m and n in Eqs. (6) and (7)] where the pump power, given by Eqs. (8) and (12), signifies the smallest power at which optical bistability can be observed. Due to the balance between the propagation losses and cumulative nonlinear effect, there is an optimal cavity length which provides a minimal threshold for optical bistability.

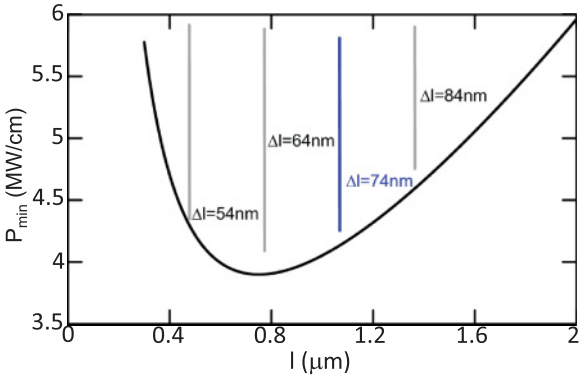

FIG. 5. (Color online) The absolute theoretical minimum of pump intensity for optical bistability $P_{\min}$ vs cavity length when $\Delta l = 54$ nm. There are also included the graphs (vertical lines) of P_+ for different stub distances Δl.

III. CONCLUSION

In summary, we suggested and verified the design of a plasmonic nanocavity made of a $\chi^{(2)}$-nonlinear material that possesses a bistable response. The nanocavity is made from a metal-insulator-metal waveguide which has been equipped with terminations made from composite stub mirrors. These composite stub mirrors are essential, and the design of each stub forming the composite mirror was purposefully chosen to be highly reflecting for either the fundamental or the second harmonic frequency, while they are transparent for the other. This allows one to compensate for any phase mismatch between the fundamental and the second harmonic by suitably adjusting the distance between the two stubs forming the composite mirror. Therefore, each involved frequency essentially experiences a cavity with a slightly deviating geometrical but equal optical length. This degree of freedom is successfully exploited to let the nanocavity sustain resonances at both involved frequencies, rendering the nonlinear conversion to be phase-matched per round trip. Using rigorous mode analysis of the waveguide with modal reflection coefficients of the nanocavity mirrors and the mean-field theory which is used to analyze the output of the nanocavity depending on the input power, it was shown that the structure can achieve optical bistability. Explicit expressions were given that allow optimization of the device such that bistability is observed at the smallest possible pump power. Taken all together, this provides a possible route to further establish the field of nonlinear plasmonics in nanocavities. This promises to be of importance in various fields of applications, e.g., for the optical computing and the routing of information in nanoplasmonic circuits that could be at the heart of future computing architecture.

ACKNOWLEDGMENTS

Support from the German Federal Ministry of Education and Research (PhoNa), by the Thuringian State Government (MeMa), and the German Science Foundation (SPP 1391 Ultrafast Nano-optics) is acknowledged.

APPENDIX: COUPLED MODE THEORY

The nonlinear evolution of modes in the waveguide is modeled within the framework of unconjugated reciprocity theorem as reported previously [18]. Assuming perturbative nonlinear polarization and monomode behavior at both FH and SH, the electromagnetic field in the waveguide can be represented as the superposition of the linear modes:

$$\mathbf{E}(x,z,t) = \sum_{\mathrm{m=F,S}} \frac{1}{2}\left[u'^{\mathrm{m}}(z,t)\mathbf{e}_0^{\mathrm{m}}(x)\exp\left(i\beta_0^{\mathrm{m}}z - i\omega_0^{\mathrm{m}}t\right) + \mathrm{c.c.}\right].$$

Slowly varying envelopes $u'(z,t)^{\{\mathrm{F,S}\}}$ describe the evolution of modes in time and the propagation direction z, while $\mathbf{e_0}^{\{\mathrm{F,S}\}}(x)$ denotes the vectorial electric field distribution in linear regime associated with the complex propagation constant $\beta_0^{\{\mathrm{F,S}\}} = \beta_0'^{\{\mathrm{F,S}\}} + i\alpha_0^{\{\mathrm{F,S}\}}/2$ at angular frequencies $\omega_0^{\{\mathrm{F,S}\}}$ for FH and SH, respectively. By using the orthogonality relations between forward- and backward-propagating modes [19] and making a first-order Taylor expansion of the dispersive propagation constant $\beta_0(\omega)$, it is straightforward to arrive at the following coupled mode equations:

$$\begin{aligned} &i\frac{\partial u'^{\mathrm{F}}}{\partial z} + \frac{i}{\nu_{\mathrm{g}}^{\mathrm{F}}}\frac{\partial u'^{\mathrm{F}}}{\partial t} + a^{\mathrm{F}}(u'^{\mathrm{F}})^{\star}u'^{\mathrm{S}}\exp\left[-\left(i\Delta\beta + \alpha_0^{\mathrm{S}}/2\right)z\right] = 0,\\ &i\frac{\partial u'^{\mathrm{S}}}{\partial z} + \frac{i}{\nu_{\mathrm{g}}^{\mathrm{S}}}\frac{\partial u'^{\mathrm{S}}}{\partial t} + b^{\mathrm{S}}(u'^{\mathrm{F}})^2\exp\left[\left(i\Delta\beta + \alpha_0^{\mathrm{S}}/2 - \alpha_0^{\mathrm{F}}\right)z\right] = 0. \end{aligned} \tag{A1}$$

Nonlinear phase mismatch is denoted by $\Delta\beta = 2\beta_0'^{\mathrm{F}} - \beta_0'^{\mathrm{S}}$, while coupling coefficients a^{F} and b^{S} have been defined using Kleinman symmetry as

$$\begin{aligned} a^{\mathrm{F}} &= \frac{\omega_0^{\mathrm{F}}\int dx\left[\bar{\bar{\chi}}^{(2)}(x) : \mathbf{e}_0^{\mathrm{F}*}(x)\mathbf{e}_0^{\mathrm{S}}(x)\right]\left[\mathbf{e}_{0\perp}^{\mathrm{F}}(x) - \mathbf{e}_{0\mathrm{z}}^{\mathrm{F}}(x)\right]}{2\int dx\left[\mathbf{e}_{0,\perp}^{\mathrm{F}}(x)\times\mathbf{h}_{0\perp}^{\mathrm{F}}(x)\right]_{\mathrm{z}}},\\ b^{\mathrm{S}} &= \frac{\omega_0^{\mathrm{S}}\int dx\left[\bar{\bar{\chi}}^{(2)}(x) : \mathbf{e}_0^{\mathrm{F}}(x)^2\right]\left[\mathbf{e}_{0\perp}^{\mathrm{S}}(x) - \mathbf{e}_{0\mathrm{z}}^{\mathrm{S}}(x)\right]}{2\int dx\left[\mathbf{e}_{0\perp}^{\mathrm{S}}(x)\times\mathbf{h}_{0\perp}^{\mathrm{S}}(x)\right]_{\mathrm{z}}}, \end{aligned} \tag{A2}$$

where $\mathbf{e}_{0\perp}^{\{\mathrm{F,S}\}}$ and $\mathbf{e}_{0\mathrm{z}}^{\{\mathrm{F,S}\}}$ are the electric field components transverse and parallel to the propagation direction, respectively. The set of Eqs. (A1) can be cast in a more simplified form by substituting $a^{\mathrm{F}} = \chi_{\mathrm{eff}}^{(2)}$, $b^{\mathrm{S}} = \gamma a^{\mathrm{F}}$ and transforming $u'^{\mathrm{F}} = u^{\mathrm{F}}/\sqrt{\gamma}e^{(\alpha_0^{\mathrm{F}}/2)z}$ and $u'^{\mathrm{S}} = u^{\mathrm{S}}e^{(\alpha_0^{\mathrm{S}}/2)z}$. This leads to

$$\begin{aligned} &i\frac{\partial u^{\mathrm{F}}}{\partial z} + \frac{i}{\nu_{\mathrm{g}}^{\mathrm{F}}}\frac{\partial u^{\mathrm{F}}}{\partial t} + i\frac{\alpha_0^{\mathrm{F}}}{2}u^{\mathrm{F}} + \chi_{\mathrm{eff}}^{(2)}u^{\mathrm{F}\star}u^{\mathrm{S}}\exp(-i\Delta\beta z) = 0,\\ &i\frac{\partial u^{\mathrm{S}}}{\partial z} + \frac{i}{\nu_{\mathrm{g}}^{\mathrm{S}}}\frac{\partial u^{\mathrm{S}}}{\partial t} + i\frac{\alpha_0^{\mathrm{S}}}{2}u^{\mathrm{S}} + \chi_{\mathrm{eff}}^{(2)}(u^{\mathrm{F}})^2\exp(i\Delta\beta z) = 0. \end{aligned} \tag{A3}$$

Equations (A3) have been straightforwardly generalized in the main article to describe the dynamism of forward- and backward-propagating modes inside a cavity.

[1] B. Prade, J. Y. Vinet, and A. Mysyrowicz, Phys. Rev. B **44**, 13556 (1991).

[2] H. Abdeldayem and D. O. Frazier, Commun. ACM **50**, 60 (2007).

[3] A. Ashkin, G. Boyd, and J. Dziedzic, IEEE J. Quantum Electron. **2**, 109 (1966).

[4] M. Liscidini and L. C. Andreani, Phys. Rev. E **73**, 016613 (2006).

[5] L. E. Myers, R. C. Eckardt, M. M. Fejer, R. L. Byer, W. R. Bosenberg, and J. W. Pierce, J. Opt. Soc. Am. B **12**, 2102 (1995).

[6] Y. Matsuzaki, T. Okamoto, M. Haraguchi, M. Fukui, and M. Nakagaki, Opt. Express **16**, 16314 (2008).

[7] W. Cai, J. S. White, and M. L. Brongersma, Nano Lett. **9**, 4403 (2009).

[8] R. Inguva and C. M. Bowden, Phys. Rev. A **41**, 1670 (1990).

[9] C. Hafner and J. Smajic, J. Mod. Opt. **58**, 467 (2011).

[10] H. P. Urbach, O. T. A. Janssen, S. van Haver, and A. J. H. Wachters, J. Mod. Opt. **58**, 496 (2011).

[11] A. Hannukainen, M. Huber, and J. Schöberl, J. Mod. Opt. **58**, 424 (2011).

[12] S. B. Hasan, R. Filter, A. Ahmed, R. Vogelgesang, R. Gordon, C. Rockstuhl, and F. Lederer, Phys. Rev. B **84**, 195405 (2011).

[13] P. B. Johnson and R. W. Christy, Phys. Rev. B **6**, 4370 (1972).

[14] R. L. Sutherland, *Handbook of Nonlinear Optics* (Marcel Dekker, New York, 1996).

[15] D. Michaelis, U. Peschel, C. Etrich, and F. Lederer, IEEE J. Quantum Electron. **39**, 255 (2003).

[16] O. Egorov, U. Peschel, and F. Lederer, Phys. Rev. E **71**, 056612 (2005).

[17] C. Etrich, U. Peschel, and F. Lederer, Phys. Rev. E **56**, 4803 (1997).

[18] Z. Ruan, G. Veronis, K. L. Vodopyanov, M. M. Fejer, and S. Fan, Opt. Express **17**, 13502 (2009).

[19] A. Snyder and J. Love, *Optical Waveguide Theory* (Springer, New York, 1983).